Chemical Engineering Journal 149 (2009) 57–69

Contents lists available at ScienceDirect

Chemical Engineering Journal

journal homepage: www.elsevier.com/locate/cej

# Mechanistic approach to intensification of sonochemical degradation of phenol

Thirugnanasambandam Sivasankar, Vijayanand S. Moholkar*

*Department of Chemical Engineering, Indian Institute of Technology Guwahati, Guwahati 781 039, Assam, India*

ARTICLE INFO

*Article history:*
Received 23 March 2008
Received in revised form
24 September 2008
Accepted 1 October 2008

*Keywords:*
Sonochemistry
Cavitation
Bubble dynamics
Advanced oxidation process

ABSTRACT

This paper addresses the matter of intensification of the sonochemical degradation of phenol from mechanistic point of view by coupling the experimental results to a mathematical model that takes into account essential physics and chemistry of cavitation bubbles. We assess the relative influence of extent of radical production by the cavitation bubbles and radical scavenging (or conservation) on the overall degradation of phenol. We have used a molecular species (oxygen) and an ionic species ($Fe^{2+}$ ions) for scavenging of radicals produced by cavitation bubbles. Four different gases, viz. argon, oxygen, nitrogen and air have been used to provide cavitation nuclei in the bulk medium. It is revealed that sonochemical degradation of phenol is governed by the extent of radical scavenging, both inside and outside the bubble. Phenomenon of radical scavenging influences the probability of interaction between the phenol molecules and radicals. The extent of degradation in the presence of $Fe^{2+}$ ions has been much higher. This result has been attributed to higher reactivity and uniform concentration of the $Fe^{2+}$ ions in the medium, as a result of which they can effectively scavenge the radicals generated by cavitation bubbles.



## 1. Introduction

A major source of water pollution is industrial wastewater discharge, which contains numerous aromatic compounds that are refractory to microorganisms. The conventional biological wastewater treatment methods, therefore, fail to completely degrade these compounds. As a result, new technologies known as advanced oxidation processes (AOPs) have been extensively explored by the researchers all over the world for effective degradation of these compounds. AOPs basically involve generation of highly reactive free radicals such as $O^{\bullet}$, $^{\bullet}OH$ and $HO_2^{\bullet}$, which are capable of initiating and accelerating the oxidation reactions leading to degradation of the aromatic pollutants. Sonochemical oxidation (or sonolysis) has been investigated as a viable AOP for the destruction of aromatic pollutants in the past one and a half decade. In this technique, the free radicals are generated through transient collapse of cavitation bubbles driven by an ultrasound wave. The possible sources of nuclei for the cavitation bubbles are tiny gas pockets trapped in the crevices of solid boundaries (such as the reactor wall) or tiny bubbles already suspended in the medium. Under the influence of pressure variation in bulk liquid due to passage of the acoustic wave, the cavitation bubble initially expands with evaporation of water at gas–liquid interface. The water vapor thus entered in the bubble condenses at the gas–liquid interface during the compression phase. At the final moments of bubble collapse, the dynamics of the bubble motion becomes extremely fast and not all of the water vapor that has evaporated in the bubble can condense. This causes entrapment of vapor molecules in the bubble. The entrapped molecules are subjected to extremes of temperature and pressure generated during transient and adiabatic collapse of the bubble and undergo dissociation generating radicals [1–3]. With fragmentation of the bubble during collapse, these radicals are released into the bulk liquid medium where they induce various chemical reactions; an example of which is the oxidation of pollutant.

The two major pathways or mechanisms for the sonolytic degradation of a pollutant are pyrolysis of the molecules evaporated inside the bubble, and secondly, the attack of $O^{\bullet}$, $^{\bullet}OH$ and $HO_2^{\bullet}$ radicals produced by the cavitation bubble (out of dissociation of water molecules during transient collapse) on the pollutant molecules in the bulk solution leading to hydroxylated products that are further degraded to the final products, i.e. $CO_2$ and $H_2O$. The principal mechanism of the degradation of the pollutant can be determined by identifying the intermediates of the degradation reaction.

One of the most ubiquitous pollutants found in wastewater of chemical and process industries is phenol. Degradation of phenol with sonolysis or sonolysis coupled with other techniques such as photocatalytic oxidation, Fenton's reagent oxidation, ozonation and peroxidation have been a subject of active research with several authors addressing the problem with different perspectives [4–22]. In these studies, the main degradation intermediates of phenol have been found to be catechol and hydroquinone, which points at attack

* Corresponding author. Fax: +91 361 2582291.
*E-mail address:* vmoholkar@iitg.ac.in (V.S. Moholkar).

1385-8947/$ – see front matter © 2008 Elsevier B.V. All rights reserved.
doi:10.1016/j.cej.2008.10.004

**Nomenclature**

| | |
|---|---|
| $c$ | velocity of sound in the liquid medium |
| $C_p$ | specific molecular heat capacity (at constant pressure) |
| $C_{p,\mathrm{mix}}$ | specific heat capacity at constant pressure of a mixture of species |
| $C_v$ | specific molecular heat capacity (at constant volume) |
| $C_{v,\mathrm{mix}}$ | specific heat capacity at constant volume of a mixture of species |
| $C_\mathrm{w}$ | concentration of water molecules in the bubble |
| $C_{\mathrm{w}0}$ | initial concentration of water molecules in the bubble |
| $C_{\mathrm{w}R}$ | concentration of water molecules at bubble interface |
| $D$ | diffusion coefficient of water vapor |
| $E$ | energy content of the bubble |
| $f$ | internal degrees of freedom for a species |
| $h$ | van der Waals hard core radius |
| $h_\mathrm{w}$ | specific molecular enthalpy of water |
| $k$ | Boltzmann constant |
| $l_\mathrm{diff}$ | mass diffusion length |
| $l_\mathrm{th}$ | thermal diffusion length |
| $m$ | molecular mass of a species |
| $n$ | concentration of a species (in molecule/m$^3$) at bubble interface |
| $N_\mathrm{Ar}$ | number of argon molecules in the bubble |
| $N_{\mathrm{N}_2}$ | number of nitrogen molecules in the bubble |
| $N_{\mathrm{O}_2}$ | number of oxygen molecules in the bubble |
| $N_\mathrm{tot}$ | total number of molecules in the bubble |
| $N_\mathrm{w}$ | number of water molecules in the bubble |
| $P_\mathrm{i}$ | pressure inside the bubble |
| $P_t$ | time variant pressure in the bulk medium driving bubble motion |
| $P_\mathrm{v}$ | vapor pressure of water |
| $Q$ | heat transferred across bubble wall |
| $r$ | radial coordinate |
| $R$ | radius of the bubble |
| $R_0$ | initial radius of the bubble |
| $T$ | temperature in the bubble |
| $t$ | time |
| $T_\mathrm{o}$ | ambient temperature in the liquid medium |
| $U_\mathrm{w}$ | specific internal energy of water molecules |
| $V$ | volume of the bubble |
| $W$ | work done by the bubble |
| $x_1, x_2$ | mole fractions of water and argon, respectively in the bubble |

*Greek letters*

| | |
|---|---|
| $\gamma$ | polytropic constant of the bubble contents |
| $\varepsilon_{\mathrm{O}_2}, \varepsilon_{\mathrm{N}_2}$ | mole fraction of oxygen and nitrogen in the bubble |
| $\eta$ | coefficient of viscosity of a species |
| $\kappa$ | thermal diffusivity |
| $\lambda$ | coefficient of thermal conductivity of a species |
| $\lambda_\mathrm{mix}$ | coefficient of thermal conductivity of the mixture of species |
| $\nu$ | kinematic viscosity of the liquid medium |
| $\rho$ | density of the liquid medium |
| $\rho_i$ | molecular density of a species |
| $\rho_\mathrm{mix}$ | molecular density of the mixture of species |
| $\sigma$ | surface tension of the liquid medium |
| $\sigma_1, \sigma_2$ | molecular diameters of water and gas, respectively |
| $\omega$ | angular frequency of pressure variation |

of $^\bullet$OH radical (i.e. hydroxylation reaction) produced by the cavitation bubbles on the phenol molecule in the bulk liquid medium as the foremost degradation pathway. However, most of the studies mentioned above have experimental approach and no attempt is made to link the results to the physics of cavitation bubbles using a suitable mathematical model. As explained in greater details in the next section, such an approach forms the basis for the study on enhancement of sonochemical degradation of phenol.

The present work addresses the matter of enhancement of the sonolytic degradation of phenol from a mechanistic perspective. With experiments under different reaction conditions coupled to a bubble dynamics model, we assess the rate of radical production from cavitation bubbles and their effective utilization for the degradation process using various scavenging techniques. We show that the rate of radical scavenging (and not the rate of radical production) is the key factor, which influences the sonochemical degradation of phenol.

## 2. Enhancement of degradation kinetics of phenol: a theoretical contemplation

Before proceeding to the description of experimental methodology, the mathematical model and results of this study, we would like to ponder over some fundamental aspects of the sonochemical degradation of phenol. The rate of the degradation reaction [Ph] + [R$^\bullet$] → [products] can be written as $-r_\mathrm{Ph} = k_\mathrm{Ph}[\mathrm{Ph}][\mathrm{R}^\bullet]$. This rate depends on the concentration of phenol molecules, [Ph], and the concentration of the radicals produced out of the cavitation bubbles, [R$^\bullet$]. Increasing any or both of these quantities should increase the rate of degradation reaction. However, as far as the sonochemical reactions are concerned, an additional factor that affects the rate and yield of the reaction, which is the probability of interaction between the reactant molecules (i.e. phenol) and the radicals. The radicals produced out of cavitation bubbles are extremely reactive. Thus, they react almost instantly after being released into the bulk medium with the transient collapse of the bubble—without diffusing significantly away in the bulk liquid medium from the location of the collapse of the bubble. Thus, the concentration of the radicals is rather localized (maximum at the interfacial region between cavitation bubble and the liquid medium) and not uniform throughout the total reaction volume. Thus, if the concentration of the reactant molecules in the vicinity of the bubble is low, the radicals may merely recombine without inducing any chemical change. An augmentation in the interaction probability results in the effective utilization of the radicals produced out of cavitation bubble and the consequent rise in the rate of degradation reaction. On this basis, one can postulate several methods of enhancing the degradation kinetics of phenol, as described below.

### 2.1. Increasing the yield of the radicals

The extent of production of radicals through cavitation bubbles depends on two factors: (1) amount of water vapor trapped in the bubble during transient collapse of the bubble and (2) the temperature peak reached in the bubble during collapse. The first factor depends on saturation (or vapor) pressure of water at the bubble–bulk interface, which in turn, decides the diffusive flux of the water molecules [23,24]. The second factor depends on the nature of gas itself. Monatomic gases like argon give very high temperature peaks during transient collapse than diatomic gases such as air, nitrogen and oxygen [25,26]. Therefore, bubbling of monatomic gas in the reaction mixture during sonication (in order to provide nuclei for cavitation events) can enhance the production

of radicals, and hence, the rate of degradation reaction. Hua and Hoffmann [27] have studied the influence of sparging of various monatomic gases on production of OH radicals during sonication.

### 2.2. Increasing the interfacial concentration of phenol

Due to hydrophobic repulsive interactions with water molecules in bulk medium, the organic molecules such as phenol are driven towards the bubble–bulk interface. This results in higher concentration of these molecules near interface than in bulk. The phenol molecules can get adsorbed onto bubble interface. This phenomenon has two consequences that contribute towards intensification of degradation of phenol: first, rise in the equilibrium vapor pressure (or partial pressure) of phenol at the gas–liquid interface that results in greater evaporation of phenol in the cavitation bubble during expansion and subsequent pyrolysis during transient collapse, and secondly, greater probability of radical–phenol interaction leading to hydroxylation of phenol as the bubble–bulk interface is also a region of high concentration of radicals. This phenomenon has been studied by Seymour and Gupta [13] and Bapat et al. [28] with different approaches. The approach of Seymour and Gupta [13] was semi-empirical. They first determined the partitioning behavior of phenol between diethyl ether and water. Proposing that the partitioning of the phenol molecules between bulk and bubble interface was proportional to partitioning in ether–water system, they described the rate of degradation of the pollutant using first order kinetic expression. The proportionality constant between ether–water and bulk–bubble interface partition coefficients was an adjustable parameter. Next, comparing the theoretically predicted and experimentally obtained degradation rates with regression analysis, Seymour and Gupta [13] showed that the phenol concentration at the bubble–bulk interface was ~3 times higher than in the bulk. On the other hand, the approach of Bapat et al. [28] was theoretical. Using the Gibb's equation for the surface excess of solute as basis [29,30], they measured the reduction in the surface tension of the aqueous solution of phenol with concentration of phenol. Correlating the slope of the plot of surface tension vs. bulk concentration to the Gibb's equation, Bapat et al. [28] determined the surface excess of phenol for bulk concentration of 0.001 M (100 ppm). Later, with simultaneous analysis of the surface concentration of phenol and water molecules at bubble–bulk interface, Bapat et al. [28] concluded that the concentration of phenol at bubble–bulk interface at equilibrium conditions would be 264 times the bulk concentration. Thus, the enrichment of phenol at bubble–bulk interface as determined by Seymour and Gupta [13] and Bapat et al. [28] differs by two orders of magnitude. However, attainment of equilibrium between bubble interface and bulk medium is difficult to achieve under transient cavitation conditions where bubble undergoes large-amplitude radial motion. The time scale of this motion is same as that of the ultrasound wave (50 μs for 20 kHz frequency). The time for the diffusion of phenol to the bubble interface through the boundary layer is expected to be several orders of magnitude higher. For representative values of boundary layer thickness as ~1 μm and diffusion coefficient of $10^{-10}$ $m^2/s$, the time scale of diffusion of phenol is ~1 ms. Due to large difference in the time scale of diffusion of phenol and the time scale of radial motion of bubble, the bubble interface is not likely to attain equilibrium (as assumed by Bapat et al. [28]) under transient cavitation conditions. The enrichment factor determined empirically by Seymour and Gupta [13], thus, seems to be more practical. Nonetheless, the above logic offers a useful tool for enhancing phenol degradation. The bubble–bulk interface is also a region with high concentration of radicals, as noted earlier. With enrichment of phenol at bubble interface, the probability of radical–phenol interaction increases significantly, resulting in an enhanced degradation through hydroxylation route. Addition of salt to the medium increases the ionic strength of the aqueous medium, and hence, the hydrophobic repulsive interactions between organic pollutant and water. This drives the phenol molecules towards the bubble–bulk interface to a greater extent and increases the degradation rates. This technique for enhancing the degradation kinetics of pollutants has been studied earlier [5,10]. Although simple and easy, this method has little practical utility for large-scale processes due to significantly large quantities of salt required. Moreover, addition of salt increases the total dissolved solids (TDS) content of the wastewater, which could give additional disposal problems.

### 2.3. Scavenging of radicals

Another possible means of raising the probability of the radical–phenol interaction is to scavenge the radicals in the bulk medium as well as inside the bubble. The word "*scavenging*" in the present context means "*conservation*", i.e. reacting the radicals with other species (present in relatively large quantities in the bubble or in the liquid medium) to generate new radical species. This prevents radical recombination, which is a loss of oxidation potential of cavitation events. Scavenging of radicals inside the bubble by other species present in the bubble (such as oxygen molecules) could result in greater release of radical species in the bulk medium. Moreover, scavenging of the radicals in the bulk medium results in penetration (or diffusion) of the radicals in the bulk medium to greater distances from the location of the collapse of cavitation bubble. Consequently, the probability of interaction of the radical with phenol molecules increases giving higher degradation rates. In this work, we have assessed the efficacy of the method of scavenging of radicals using a molecular ($O_2$) and an ionic ($Fe^{2+}$) species coupled with the technique of sparging monatomic and diatomic gases through the reaction medium for the enhancement of the degradation of phenol. As noted earlier, dissociation of water molecules trapped in the cavitation bubble results in the generation of radical species such as $H^\bullet$, $^\bullet OH$ and $HO_2^\bullet$.

#### 2.3.1. Oxygen scavenging

Oxygen present in the bubble (in gaseous form) and present in the medium (in dissolved or aqueous form as well as in the form of tiny bubbles suspended in the medium) can scavenge radicals inside the bubble as well as in the bulk medium in several ways. Dissociation of molecular oxygen in the bubble influences the formation of $^\bullet OH$ radicals via reactions:

$$O_2 \rightleftharpoons 2O^\bullet \quad \text{(R.1)}$$

$$O^\bullet + H_2O \rightleftharpoons 2{}^\bullet OH \quad \text{(R.2)}$$

It should be noted that the second reaction could also occur in the bulk medium where $O^\bullet$ radicals released in the medium with transient collapse of the bubble can react with water molecules to generate additional $^\bullet OH$ radicals. The oxygen in the bubble can also react with $H^\bullet$ radicals formed out of water dissociation to generate $^\bullet OH$ and $HO_2^\bullet$ radicals via following reactions:

$$H_2O \rightleftharpoons H^\bullet + {}^\bullet OH \quad \text{(R.3)}$$

$$H^\bullet + O_2 \rightleftharpoons O^\bullet + {}^\bullet OH \quad \text{(R.4)}$$

$$H^\bullet + O_2 \rightleftharpoons HO_2^\bullet \quad \text{(R.5)}$$

Reactions (R.4) and (R.5) can also occur in bulk liquid medium where dissolved oxygen can react with $H^\bullet$ radicals released during transient bubble collapse generating additional oxidizing species. In addition to this, the dissolved oxygen in the medium can help revert the loss of oxidation potential due to recombination of $^\bullet OH$

radicals released in the medium by generating $HO_2^{\bullet}$ species as follows:

$$^{\bullet}OH + {}^{\bullet}OH \rightleftharpoons H_2O_2 \quad (R.6)$$

$$H_2O_2 + O_2 \rightleftharpoons 2HO_2^{\bullet} \quad (R.7)$$

Finally, the dissolved oxygen can also react with $^{\bullet}OH$ radicals released in the medium to generate additional oxidizing species:

$$^{\bullet}OH + O_2 \rightleftharpoons HO_2^{\bullet} + O^{\bullet} \quad (R.8)$$

If any other reactive species (in addition to water vapor and oxygen) is present in the bubble (for example nitrogen in case of air bubbles), the scavenging action of oxygen is influenced as the additional species competes with oxygen. This point is discussed in greater detail later in the paper.

#### 2.3.2. $Fe^{2+}$ scavenging

Being an ionic species, the scavenging action of $Fe^{2+}$ is restricted only in the bulk liquid medium and not inside the bubble. $Fe^{2+}$ ions react with the hydrogen peroxide formed out of recombination of $^{\bullet}OH$ radicals released in the medium with transient collapse of cavitation bubbles. Thus, $Fe^{2+}$ reverts the loss of oxidation potential of cavitation bubbles. In the process, $Fe^{2+}$ is oxidized to $Fe^{3+}$ as per following reactions:

$$^{\bullet}OH + {}^{\bullet}OH \rightleftharpoons H_2O_2 \quad (R.6)$$

$$H_2O_2 + Fe^{2+} \rightarrow Fe^{3+} + OH^- + {}^{\bullet}OH \quad (R.9)$$

It must be noted that there are two sources of hydrogen peroxide in the medium. First, the $H_2O_2$ produced due to recombination of radicals per reaction (R.6). Secondly, $H_2O_2$ is also formed in the bubble, in equilibrium proportion, due to dissociation of water molecules. However, the equilibrium fraction of $H_2O_2$ among various species in the bubble at the moment of collapse is usually very small. Thus, the main scavenging action of $Fe^{2+}$ is due to its reaction with $H_2O_2$ formed due to recombination of $^{\bullet}OH$ radicals. $Fe^{2+}$ ions are regenerated in the medium by following reactions:

$$Fe^{3+} + H_2O_2 \rightarrow Fe^{2+} + HO_2^{\bullet} + H^+ \quad (R.10)$$

$$Fe^{3+} + HO_2^{\bullet} \rightarrow Fe^{2+} + O_2 + H^+ \quad (R.11)$$

Due to continuous regeneration, the average concentration of $Fe^{2+}$ in the bulk medium stays very nearly constant. Due to this feature, $Fe^{2+}$ can provide effective scavenging of radicals.

## 3. Experimental

### 3.1. Reagents

The reagents used in the present study are as follows: phenol (Merck, Grade: Synthesis), iron (II) sulphate heptahydrate (Merck, Grade: Purified), acetonitrile (Merck, Grade: HPLC) and water (Merck, Grade: HPLC). All reagents were used as received. The aqueous solution of phenol with bulk concentration of 0.001 M or 100 ppm (typical of the concentration levels in industrial wastewater discharge) was prepared using Elix water from Millipore® purification unit (Model: Elix 3). Four gases, viz. oxygen, argon, nitrogen and air (99.99% purity) were used for bubbling the reaction solution.

### 3.2. Experimental setup

A schematic diagram of the experimental setup used in the present study is shown in Fig. 1. A microprocessor-based and programmable ultrasound processor (Sonics and Materials Inc., Model VCX 500) was used for sonication of the phenol solution. The frequency of the processor was 20 kHz with maximum power output of 500 W. The ultrasound probe of the processor was fabricated from high-grade titanium alloy and had a tip diameter of 13 mm. With a variable power output control, the net consumption of power during sonication was set at 100 W (20% of the maximum value). The actual value of the ultrasound intensity in the medium was determined using calorimetry [31]. For a power output of 100 W the ultrasound probe produced an acoustic wave with 1.5 kPa amplitude. The processor had facility of automatic frequency tuning and amplitude compensation, which ensures constant power delivery to the ultrasound probe irrespective of the changes occurring in the liquid medium during degradation process. For the sonication of the phenol solution, a jacketed glass reactor (dimensions: height, 120 mm; diameter, 50 mm; jacket diameter, 62 mm) was used. This reactor was positioned on a laboratory jack, which could be raised or lowered for exact positioning of the ultrasound probe in the solu-

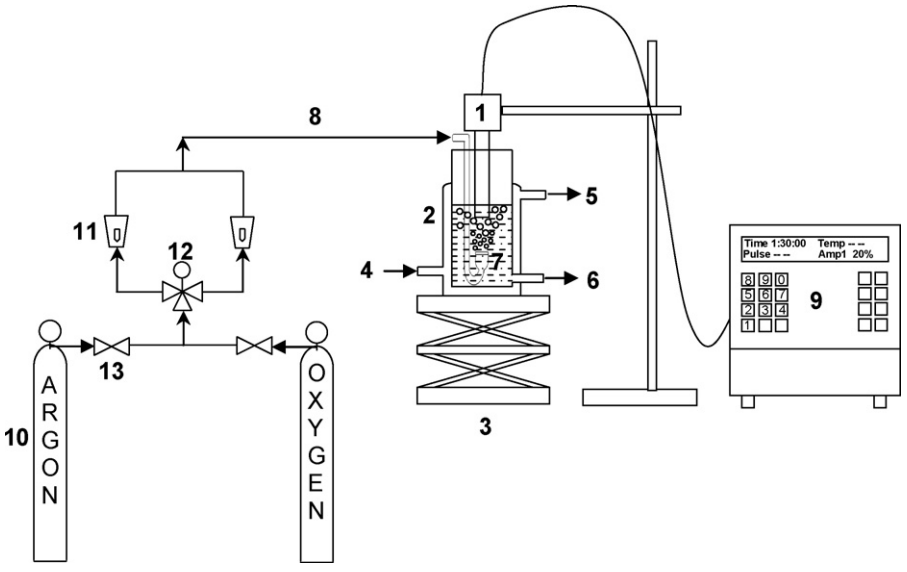


**Fig. 1.** Schematic diagram of the experimental setup. Legends: 1, ultrasound horn; 2, jacketed glass reactor; 3, laboratory jack; 4, cooling water inlet; 5, cooling water outlet; 6, sample port; 7, aerator; 8, gas inlet; 9, control unit of ultrasonic processor; 10, gas cylinder; 11, rotameter; 12, three-way valve and 13, gas flow controlling valve.

tion. The tip of the ultrasound probe was placed 15 mm below liquid surface so as to ensure effective coupling between tip of the horn and the bulk liquid medium. For bubbling of the gas in the reaction solution, a glass sparger was used. This sparger had silica filter (pore size ~40 μm) to disperse gas in the solution in the form of fine bubbles. The sparger was so positioned that the porous silica filter exactly faces the bottom of the ultrasound probe. This feature helps uniform distribution of gas bubbles forming cavitation nuclei in the solution. The distance between ultrasound probe tip and silica filter was fixed at 20 mm. The flow of gas to the sparger was controlled using a three-way valve connected to two rotameters, as shown in Fig. 1.

### 3.3. Experimental procedure and analysis

#### 3.3.1. Sonochemical degradation experiments

150 mL of phenol solution with 0.001 M (100 ppm) concentration at an initial temperature of 298 K was used for sonication. The total sonication time in all experiments was 5400 s (90 min); however, in order to avoid significant rise in the temperature of the solution the sonication was done in pulse mode with sonication period of 900 s (15 min) followed by a silent period of 300 s (5 min). In addition, cooling water was circulated through the jacket during sonication in order to maintain the temperature of the reaction medium constant. The temperature of the solution was monitored continuously during sonication with a digital thermometer. The rise in the temperature of solution during experiment was ~2 K. The experiments were categorized as follows:

(1) Sonication of phenol solution with continuous bubbling of either of the four gases (viz. nitrogen, air, oxygen and argon) at a flow rate of $1.389 \times 10^{-3}$ mL/s (5 L/h).
(2) Sonication of phenol solution with bubbling of either argon or nitrogen at flow rate of $1.389 \times 10^{-3}$ mL/s (5 L/h) during the 900-s (15 min) sonication period and bubbling of oxygen during 300 s (5 min) silent period at a flow rate of $2.778 \times 10^{-3}$ mL/s (10 L/h).
(3) Sonication of phenol solution with continuous bubbling of any of the four gases mentioned above with 0.5 mM $FeSO_4 \cdot 7H_2O$ added to the solution.

Addition of $FeSO_4 \cdot 7H_2O$ can increase the ionic strength of the medium, and hence, the repulsive hydrophobic interactions of phenol with water molecules. As a result, the partitioning of phenol between bulk and interface can rise; and the interfacial concentration of phenol increases. This effect can enhance degradation of phenol. However, this effect is observed principally for $FeSO_4$ addition in moderate to high concentrations. In order to isolate this effect, the $FeSO_4$ addition in the present experiments has been kept quite low; i.e. at a concentration of 0.5 mM. Moreover, it needs to be mentioned that the solubility of the four gases used in this study differs. The solubilities of the gases in water at the temperature of experiment are as follows: $N_2 = 0.6$ mol/m$^3$, Ar = 1.4 mol/m$^3$, $O_2 = 1.3$ mol/m$^3$ and Air = 0.794 mol/m$^3$. It is likely that some of the gas being sparged through the solution will dissolve in water, without forming cavitation nuclei. However, the rate of sparging (or bubbling) of all four gases was $3.33 \times 10^{-3}$ mol/s (5 L/h), which is rather high compared to the solubilities. As a result, the bulk medium gets saturated with the gas within short time. Thereafter, all of the gas entering the medium is essentially utilized for the nucleation of cavitation events. Some loss of phenol from the solution may also occur due to diffusion (or stripping) with the gas sparged through the solution. This loss may be misinterpreted as degradation. In order to assess this loss, the final phenol concentration in the solution with 0.001 M (100 ppm) initial concentration was measured after sparging of $N_2$, $O_2$, air and argon at a rate of $1.389 \times 10^{-3}$ mL/s (5 L/h) for 5400 s (90 min); in the absence of ultrasound irradiation. The final concentration of phenol was practically same as initial concentration. This result shows that no loss of phenol occurs due to diffusion (or stripping) with bubbling gas. A simple explanation for this result can be given as follows: the vapor pressure of phenol in pure form at the temperature of the experiment (298 K) is mere ~40 Pa. The concentration of phenol in the solution is very low (0.001 M or 100 ppm). Therefore, the equilibrium vapor pressure or partial pressure of phenol in 0.001 M (100 ppm) solution, as determined by Raoult's law, is negligibly small ~0.04 Pa. Hence, practically no diffusion of phenol occurs with sparging of gas through the solution.

All experiments were done in triplicate to assess the reproducibility of the results. The mean of the percentage degradation obtained in three experimental runs was taken into consideration for further analysis. The final concentration of phenol in the solution after 5400 s (90 min) of sonication was determined using HPLC (PerkinElmer, Model: Series 200). A C18 column (Make, Chromatopak, dimensions: 250 mm × 4.6 mm, particle size of packing: 5 μm) was used with a mixture of acetonitrile:water (80:20) as the eluent. The flow rate of eluent was maintained at $1.67 \times 10^{-2}$ mL/s with sample injection volume being 20 μL. The UV detector wavelength for phenol was 275 nm. We would like to categorically state that we have not made an analysis of the intermediate products of degradation of phenol as these have been well studied and documented in the literature mentioned earlier. We have monitored the rate of disappearance of original pollutant and the analysis has been made on that basis.

#### 3.3.2. Dissolved species variation

In another experiment, changes in the dissolved oxygen content of Elix water with sparging of nitrogen and argon was studied. For this purpose, the desired gas (either nitrogen or argon) was sparged through water initially saturated with oxygen in a 100-mL beaker using the gas sparger at a flow rate of $1.389 \times 10^{-3}$ mL/s (5 L/h). During bubbling, the water was stirred using a magnetic stirrer. The dissolved oxygen concentration was monitored using a DO meter (Make, Consort, Model: C863). To assess the influence of sonication on the removal of dissolved oxygen with sparging of argon and nitrogen, this experiment was also conducted with simultaneous irradiation of ultrasound.

## 4. Mathematical formulation

In the context of the present study, the problem of mathematical modeling comprises of simulating the radial motion of cavitation bubbles comprising of various gases (viz. nitrogen, argon, oxygen and air) with the accompanying heat transfer and evaporation/entrapment of vapor molecules, and finally determine the various chemical species that result out of transient collapse of the bubble. This subject has been an active area of research for the past 3 decades and various authors have dealt with the matter with different approaches [32–38]. The most general treatment of the problem of vapor transport in large amplitude nonlinear motion of the cavitation bubbles was presented by Storey and Szeri [23]. The principal result of analysis of Storey and Szeri [23] was that vapor transport in the bubble is a diffusion-limited process. In view of these conclusions, Toegel et al. [24] developed a diffusion-limited ODE model using boundary layer approximation [39–42], which forms the basis of the model of this paper. This model has been validated against the full PDE simulations of Storey and Szeri [23]. It should be noted that the overall degradation of phenol is a manifestation of simultaneous oscillations of millions of bubbles present in the bulk liquid medium. In such a system numerous factors such a

bubble–bubble coalescence, clustering, rectified diffusion affect the overall sonochemical yield, i.e. the extent of degradation of phenol. In addition to this, the number density of bubbles is also a crucially important parameter. No experimental method has been developed yet, which can provide an estimate of this parameter, even with an order of magnitude accuracy. No model for the radial motion of a cavitation bubble has been developed so far, which takes into account all of these facets. Research in the area of radial motion of bubble has been restricted mostly to analysis of single bubbles. The single bubble models do not address the entire physical phenomena in the system, yet they provide a qualitative physical insight into the problem, as these models address the essential physics of the problem such as heat transfer, mass transfer, vapor entrapment, etc.

Attempts of modeling physical or chemical effects of multi-bubble systems with single bubble models have been made by earlier authors. Ilyichev et al. [43] have shown that all spectral characteristics of experimental acoustic cavitation (involving multi-bubble fields) can be explained with simulations of a single bubble. Prasad Naidu et al. [33] and Rajan et al. [44] have successfully explained the trends in the sonochemical oxidation of water–KI and water–KI–$CCl_4$ system using single bubble model. More recently, Storey and Szeri [45] have pointed out that experimentally observed trends in sonochemistry are reflected in the trends observed in the behavior of a single representative bubble. However, the principal limitation of the single bubble models (due to the approximations in them) is that *no quantitative* predictions about reaction kinetics and yield can be made with them.

As far as objectives of the present study are concerned, single bubble approach for mathematical modeling is sufficient.

### 4.1. Bubble dynamics model

The bubble motion is described by Keller–Miksis equation [46,47] as

$$\left(1-\frac{dR/dt}{c}\right)R\frac{d^2R}{dt^2}+\frac{3}{2}\left(1-\frac{dR/dt}{c}\right)\left(\frac{dR}{dt}\right)^2 = \frac{1}{\rho}\left(1+\frac{dR/dt}{c}\right)(P_i-P_t)+\frac{R}{\rho c}\frac{dP_i}{dt}-4\nu\frac{dR/dt}{R}-\frac{2\sigma}{\rho R} \quad (1)$$

where $P_t$ is the time variant pressure in the bulk liquid driving bubble motion. The pressure inside the bubble, $P_i$ is written as:

$$P_i = \frac{N_{tot}(t)kT}{\left[(4\pi/3)(R^3(t)-h^3)\right]} \quad (2)$$

where $h \sim R_0/8.86$ is the van der Waals hard core radius determined by the excluded volume of gas molecules. Since the hard core radii of the species considered in the present work viz. nitrogen, oxygen, water and argon differ only by a small magnitude, we take a common value for the hard-core radius. Eq. (1) can be easily transformed into two simultaneous ODEs by following substitution:

$$\frac{dR}{dt} = s \quad (3)$$

$$\frac{ds}{dt} = \frac{(1+s/c)}{R\rho(1-s/c)}(P_i-P)+\frac{1}{\rho c(1-s/c)}\frac{dP_i}{dt}-\frac{4\nu s}{R^2(1-s/c)} -\frac{2\sigma}{\rho R^2(1-s/c)}-\frac{3s^2(1-s/3c)}{2R(1-s/c)} \quad (4)$$

### 4.2. Heat and mass transfer across bubble

Both gas and vapor (of phenol and water) diffuse across the bubble wall during radial bubble motion. The time scale of gas diffusion can be given as $\sim R_0^2/D$ where $R_0$ is the initial radius of the bubble ($\sim$10 μm) and $D$ is the diffusion coefficient ($\sim 10^{-9}$ m$^2$/s). Thus, the time scale of gas diffusion becomes $\sim$0.1 ms, which is much higher than the time scale of radial bubble motion (which is same as time scale of ultrasound wave: 50 μs for 20 kHz wave). Thus, the transport of gas across the bubble during radial motion can be ignored.

The equilibrium vapor pressure or partial pressure of phenol in the bulk medium (with concentration of 0.001 M or 100 ppm) is 0.04 Pa, as noted earlier. Due to hydrophobic repulsive interactions, enrichment of phenol occurs at the bubble–bulk interface, and the concentration of phenol is $\sim$3 times the bulk concentration. Despite this, the partial pressure of phenol at the bubble–bulk interface is $\sim$0.12 Pa, which is several orders of magnitude smaller than partial pressure of water. Due to very low partial pressure, the evaporation of phenol into the bubble during expansion is negligible and can be ignored. Diffusion of water vapor into the bubble, as a result of evaporation occurring at the bubble interface needs to be taken into account, nonetheless.

The temperature inside the bubble exceeds the surface temperature of the bubble (which is same as bulk liquid temperature) only for a very brief moment during collapse. On the basis of this condition, the bubble can be divided into two parts: (1) a "cold" boundary layer in thermal equilibrium with the liquid, and (2) a hot homogeneous core. An underlying assumption in this hypothesis is that the condensation of water molecules at the bubble wall is fast enough to maintain equilibrium phase change. By dimensional analysis, the instantaneous diffusive penetration depth is given by: $l_{diff} = \sqrt{Dt_{osc}}$, where $t_{osc}$ is the time scale of bubble oscillations, $R/|dR/dt|$. The rate of change of water molecules in the bubble by diffusion is given by

$$\frac{dN_w}{dt} = 4\pi R^2 D\frac{\partial C_w}{\partial r}\bigg|_{r=R} = 4\pi R^2 D\left(\frac{C_{wR}-C_w}{l_{diff}}\right) \quad (5)$$

where $C_{wR}$ is the equilibrium concentration of water molecules at the bubble wall, and it is calculated from the equilibrium vapor pressure at the bubble wall corresponding to bulk liquid temperature. $C_w$ is the actual concentration of water molecules in the bubble core. The diffusion coefficient for the transport of water vapor has been determined using the Chapman–Enskog theory using Lennard–Jones 12-6 potential [51–53]. For greater details on calculation of diffusion coefficient, we refer the readers to our earlier papers [48,49].

With complete analogy with mass transfer, the heat transfer across bubble wall is given by

$$\frac{dQ}{dt} = 4\pi R^2\lambda\left(\frac{T_o-T}{l_{th}}\right) \quad (6)$$

where $\lambda$ is the thermal conductivity of the bubble contents and $l_{th}$ is the thermal diffusion length written as $l_{th} = \sqrt{\kappa t_{osc}}$. The thermal diffusivity, $\kappa$ of the gas–vapor mixture in the bubble is calculated as $\kappa = \lambda/\rho_{mix}C_{p,mix}$, where $\rho_{mix}C_{p,mix} = \sum_i \rho_i C_{pi}$. $\rho_i$ are the densities of the species present in the bubble (in molecule/m$^3$) and $C_{pi}$ are the molecular specific heats of these species. Values of $C_{pi}$ for various species are listed in Table 1. The effective thermal conductivity of the bubble contents (mixture of gas and water vapor) has been calculated using a semi-empirical method [50]. This method uses the thermal conductivity of the individual components, which has been calculated using Chapman–Enskog theory using Lennard–Jones 12-6 potential [51–53], with Eucken correction applied for polyatomic

**Table 1**
Thermodynamic properties of various species.

| Species | Degree of freedom ($f$) | Molecular specific heat ($C_p$) | Molecular specific heat ($C_v$) |
|---|---|---|---|
| $N_2$ | 5 | $\frac{7}{2}k$ | $k\left(\frac{5}{2}+\frac{(\theta_{N_2}/T)^2\exp(\theta_{N_2}/T)}{(\exp(\theta_{N_2}/T)-1)^2}\right)$ |
| $O_2$ | 5 | $\frac{7}{2}k$ | $k\left(\frac{5}{2}+\frac{(\theta_{O_2}/T)^2\exp(\theta_{O_2}/T)}{(\exp(\theta_{O_2}/T)-1)^2}\right)$ |
| $H_2O$ | 6 | $4k$ | $k\left(3+\sum_i^3 \frac{(\theta_{i,H_2O}/T)^2\exp(\theta_{i,H_2O}/T)}{(\exp(\theta_{i,H_2O}/T)-1)^2}\right)$ |
| Ar | 3 | $\frac{5}{2}k$ | $\frac{3}{2}k$ |

*Note*: $\theta_i$s are the vibrational temperatures of various species: $\theta_{N_2}=3350$ K, $\theta_{O_2}=2273$ K, $\theta_{1,H_2O}=2295$ K, $\theta_{2,H_2O}=5255$ K, $\theta_{3,H_2O}=5400$ K.

molecules. For greater details on this, we refer the readers to our earlier papers [48,49].

#### 4.2.1. Limits on the diffusion length

At the instances of maximum and minimum radius, the bubble wall velocity is zero, and thus, an alternate expression is needed for diffusion length. We set this limit as $R/\pi$ after identifying that vapor transport is governed by pure diffusion equation for condition $dR/dt=0$. The limit $R/\pi$ is set on the basis of solution of the diffusion equation in spherical geometry. For greater details on this, we refer the reader to our earlier papers [48,49]. Thus, the expressions for the mass and thermal diffusion length are given as

$$l_{\text{diff}} = \min\left(\sqrt{\frac{RD}{|dR/dt|}}, \frac{R}{\pi}\right) \tag{7}$$

$$l_{\text{th}} = \min\left(\sqrt{\frac{R\kappa}{|dR/dt|}}, \frac{R}{\pi}\right) \tag{8}$$

We would like to mention that the bubble dynamics model of Yasui [34] relaxes the assumption of cold boundary layer. The temperature of the bubble–bulk interface calculated with this approach exceeds 10,000 K. This temperature is sufficient to cause pyrolytic degradation of phenol present in the interfacial region. However, this extreme condition lasts for very short time duration, typically 10 ns or so, at the instance of maximum compression in radial bubble motion. The kinetics of phenol pyrolysis is expected to be much slower, typically in the range of milliseconds. As a consequence of this limitation, practically no degradation of phenol is expected to occur through the route of pyrolysis in bubble–bulk interfacial region.

### 4.3. Overall energy balance

During radial motion, both heat and mass transfer occurs across the bubble wall, and thus, the overall energy balance for the bubble contents is written as

$$\frac{dE}{dt} = \frac{dQ}{dt} - \frac{dW}{dt} + h_w\frac{dN_w}{dt} \tag{9}$$

The total energy $E$ of the bubble is a function of temperature and volume of the bubble and the number of molecules of various gas and vapor species in it. In the present study, we use four gases for bubbling the reaction mixture, viz. argon, nitrogen, oxygen and air. The first three gases are single component gases, while air is a two-component (nitrogen and oxygen) gas. Therefore, the energy balance for the bubbles of single component gas and air needs to be written separately:

(1) Argon/nitrogen/oxygen bubble:

$$\frac{dE}{dt} = \left(\frac{\partial E}{\partial N_G}\right)_{N_w,V,T}\frac{dN_G}{dt} + \left(\frac{\partial E}{\partial N_w}\right)_{N_G,V,T}\frac{dN_w}{dt} + \left(\frac{\partial E}{\partial T}\right)_{N_w,N_G,V}\frac{dT}{dt} + \left(\frac{\partial E}{\partial V}\right)_{N_w,N_G,T}\frac{dV}{dt} \tag{10}$$

where $N_G$ denotes molecules of the gas (G = $N_2$, $O_2$ or Ar).

(2) Air bubble:

$$\frac{dE}{dt} = \left(\frac{\partial E}{\partial N_{N_2}}\right)_{N_w,N_{O_2},V,T}\frac{dN_{N_2}}{dt} + \left(\frac{\partial E}{\partial N_{O_2}}\right)_{N_{N_2},N_w,V,T}\frac{dN_{O_2}}{dt} + \left(\frac{\partial E}{\partial N_w}\right)_{N_{N_2},N_{O_2},V,T}\frac{dN_w}{dt} + \left(\frac{\partial E}{\partial T}\right)_{N_w,N_{N_2},N_{O_2},V}\frac{dT}{dt} + \left(\frac{\partial E}{\partial V}\right)_{N_w,N_{N_2},N_{O_2},T}\frac{dV}{dt} \tag{10a}$$

where $N_{N_2}$ and $N_{O_2}$ are the number of molecules of nitrogen and oxygen, respectively in the bubble. As we neglect the change in the gas content of the bubble for the reasons stated earlier, $dN_G/dt=0$ for single component gas and $dN_{N_2}/dt = dN_{O_2}/dt = 0$ for air. The term $dN_w/dt$ is the rate of change of water vapor content of the bubble and is evaluated according to Eq. (5). The specific enthalpy of the water molecules entering the bubble from cold bubble interface is $h_w = 4kT_o$. The specific energy of the water molecules in the bubble is the thermal energy, and is written in terms of vibrational temperatures as

$$\left(\frac{\partial E}{\partial N_w}\right) = U_w = N_w kT\left(3+\sum\frac{\theta_i/T}{\exp\left(\theta_i/T\right)-1}\right) \tag{11}$$

The work done by the bubble is the expansion work: $P_i dV$. Moreover, $(\partial E/\partial T) = C_v$ and $(\partial E/\partial V) = 0$, as the internal energy of an ideal gas mixture is a function of its temperature and composition. With inclusion of various terms above in the overall energy balance, we obtain an equation for the change in the temperature of the bubble as

$$C_{v,\text{mix}}\frac{dT}{dt} = \frac{dQ}{dt} - P_i\,dV + (h_w - U_w)\frac{dN_w}{dt} \tag{12}$$

The specific heat of the gas–vapor mixture ($C_{v,\text{mix}}$) present in the bubble is written as

$$C_{v,\text{mix}} = \sum_i C_{v,i}N_i \quad \text{where } i = N_2/O_2/\text{Ar/Air and } H_2O \tag{13}$$

where $C_{v,i}$ is the molecular specific heat of species $i$, and $N_i$ is the number of molecules of that species present in the bubble. The $C_v$ values for the various species considered in this work are listed in Table 1.

### 4.4. Numerical solution

The Eqs. (1), (5), (6) and (12) constitute complete formulation for the radial motion of cavitation bubble with associated heat and mass transfer effects. This set of simultaneous ODEs can be solved using Runge–Kutta 4th order–5th order adaptive step size method [54]. The cavitation bubble may collapse at the instance of maximum compression during radial motion. The word "collapse" essentially means fragmentation of the cavitation bubble. This phenomenon depends on many factors such as shape (or surface) instability of bubbles, the local flow conditions and the bubble population density in the vicinity of the bubble. For conditions of maximum shape and flow instability, the cavitation bubble fragmentation can occur at the first compression after an initial expansion. In view of this, the condition for the bubble collapse is taken to be first compression during radial motion. Four important parameters required for the simulation of the radial motion of the cavitation bubble are (1) frequency and (2) pressure amplitude of ultrasound, (3) vapor pressure of water and (4) initial (or equilibrium) bubble radius. Numerical values for these parameters have been determined as follows:

(1) *Frequency*: The frequency of the ultrasound wave was taken as 20 kHz, which is the frequency of the sonicator used in the experiments.
(2) *Pressure amplitude*: A calorimetric method was used to determine the amplitude of the ultrasound wave emitted by the sonicator probe [31]. The amplitude of the ultrasound wave generated by the sonicator probe was 1.5 kPa. However, the actual pressure amplitude sensed by the cavitation bubble located away from the probe tip is lesser than 1.5 kPa, as the ultrasound wave attenuates during propagation through the medium. This attenuation varies directly with the viscosity of the medium and the size and population density of bubbles in the medium [55,56]. A direct measurement of the local pressure amplitude in the vicinity of the cavitation bubble is beyond the capabilities of the instrumentation used in the present study. Therefore, we assume about 15% attenuation and use a value of 1.3 kPa for acoustic pressure amplitude in the numerical simulations.
(3) *Vapor pressure of water*: The vapor pressure of the bulk medium (i.e. water) was calculated with Antoine's equation using initial temperature of the solution (298 K). The temperature rise during sonication was ~2 K, as noted earlier. The difference between vapor pressure of water at 298 and 300 K is quite small (<10%). Therefore, we have ignored the temperature rise during simulations, assuming the liquid medium at constant temperature. An alternate approach would be to calculate the vapor pressure of water using average of initial and final temperatures. However, this would make trivial quantitative changes to the simulation results.
(4) *Initial (or equilibrium) bubble radius*: This parameter is difficult to estimate. Moreover, the equilibrium size of the bubble keeps on changing due to phenomena such as rectified diffusion, fragmentation of the bubble etc. The minimum radius of the cavitation nuclei which would grow into a bubble for particular amplitude of acoustic wave can be determined by the analysis given by Young [57]. For the acoustic pressure amplitude in the present experiments, this value is ~2 μm. As mentioned earlier, a gas sparger distributing the desired gas through a glass frit with pore size of ~40 μm was used to provide cavitation nuclei. The gas bubbles generated out of the glass frit would of the same size as that of the pore. However, these bubbles get shattered into multiple fragments with wide size distribution due to ultrasound. We have chosen a representative value of 10 μm for the initial or equilibrium bubble radius.

Moreover, the initial water vapor content of the bubble (of all four gases) is taken to be zero in the simulations. In other words, initially (at $t = 0$) the cavitation bubble is assumed to be comprised of gas alone.

Equilibrium composition of the various species formed in the bubble at transient collapse due to the dissociation of entrapped water molecules was calculated with software FACTSAGE that employs the free-energy minimization algorithm proposed by Eriksson [58] using values of temperature and pressure peak reached in the bubble at the first compression. This software has an in-built database of $C_p$ vs. temperature relationship, entropy and heat of formation of all the above species. A more rigorous approach in this regard would be to include various radical reactions in the mass balance equations along with heats of these reactions included in the energy balance [23,59,60]. Endothermicity of some of the radical reactions (for example $H_2O \rightleftharpoons H^{\bullet} + {}^{\bullet}OH$) works towards lowering of the peak temperature reached during transient bubble collapse. However, addition of this feature in the present model would change only the final quantitative answers, with trends remaining essentially unaltered.

## 5. Results and discussion

The concentration of phenol in the aqueous solutions used in the present study is 100 ppm, which is rather dilute. Therefore, the probability of interaction between phenol molecules and radicals becomes a crucial parameter influencing the kinetics of degradation. For such a situation, significant fraction of the radicals generated out of cavitation bubbles may undergo recombination without reacting with the phenol molecules. Therefore, merely increasing the rate of production of radicals may not give required enhancement in degradation rates. The radicals generated out of cavitation bubbles need to be scavenged in order to raise the probability of their interaction with phenol molecules. As stated earlier, the word *scavenging* means *conservation*, i.e. generation of new radicals by reacting the radicals with other species in the medium, such as dissolved oxygen. The extent of radical scavenging in the medium depends on the concentration of the scavenging species in the bulk liquid medium. This concentration needs to be maintained uniform throughout the sonication period (nearly to the saturation level) in order to achieve effective scavenging leading to greater degradation. With this preface, we present the results of the experiments and simulation of radial bubble motion.

Trends in the degradation of phenol obtained in three categories of experiments are shown in Fig. 2. The variation in the dissolved oxygen content of Millipore water with bubbling of nitrogen and argon is shown in Fig. 3. Simultaneous irradiation of ultrasound, in addition to bubbling of nitrogen and argon, did not make any noticeable change to the rate of reduction in the dissolved oxygen in the solution. An explanation for this result can be given in terms of difference in the time scale of bubbling of gases and the time scale of ultrasound irradiation. The time scale of sparging of the gas (nitrogen and argon at the flow rate of $1.389 \times 10^{-3}$ mL/s or 5 L/h) is in seconds, while the time scale of ultrasound is in microseconds, which is six orders of magnitude smaller. Due to such large difference in the time scale of two processes, the removal of dissolved oxygen in the medium is principally influenced by the sparging of

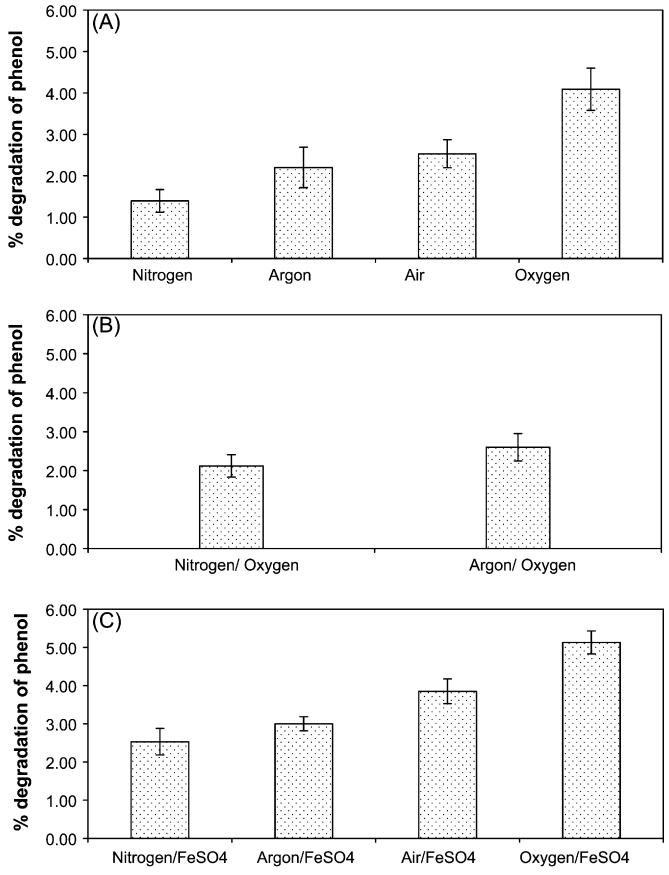


**Fig. 2.** Experimental results on the degradation of phenol in various categories of experiments. (A) Sonication of phenol solution with continuous bubbling of either of the four gases (viz. nitrogen, air, oxygen and argon). (B) Sonication of phenol solution with bubbling of either argon or nitrogen during sonication period and bubbling of oxygen during silent period. (C) Sonication of phenol solution with continuous bubbling of either of the four gases with $FeSO_4{\cdot}7H_2O$ added to the solution.

gas, with no effect of ultrasound irradiation. The highest degradation of phenol is obtained with bubbling of oxygen through reaction mixture with $FeSO_4{\cdot}7H_2O$ added to the solution; while the lowest degradation is seen for nitrogen as the bubbling gas. Some other salient features of the experimental results are as follows:

(1) The degradation obtained with bubbling of air and argon through reaction mixture is almost similar.

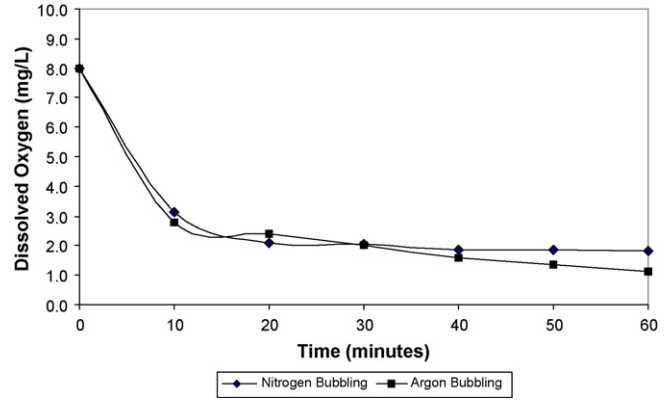


**Fig. 3.** Reduction in the dissolved oxygen content of Millipore water with continuous bubbling of nitrogen and argon.

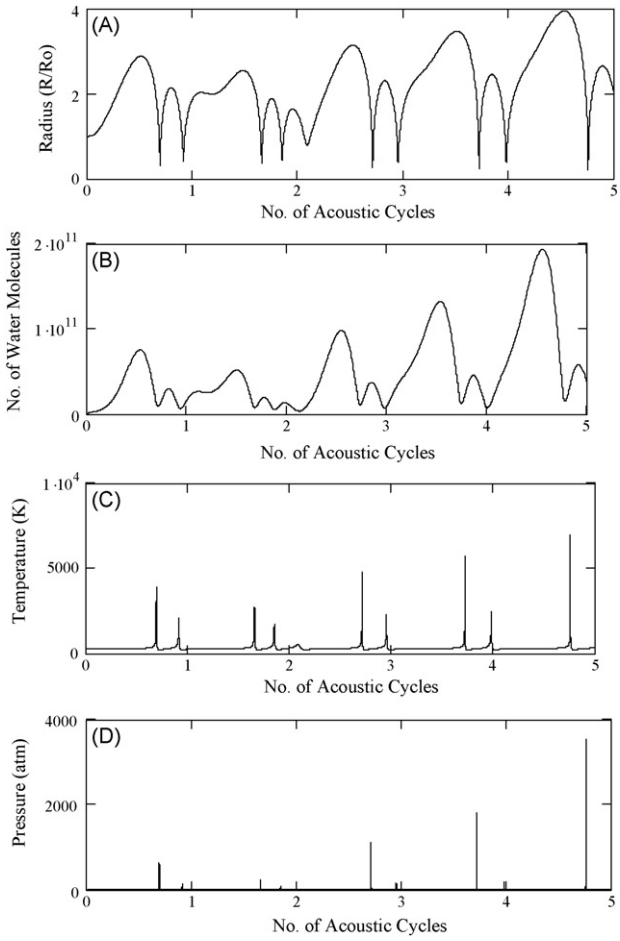


**Fig. 4.** Simulation of the radial motion of 10 μm argon bubble in the 100-ppm aqueous solution of phenol. Time variation of (A) normalized bubble radius ($R/R_0$); (B) number of water molecules in the bubble; (C) temperature in the bubble and (D) pressure inside the bubble.

(2) With alternate bubbling of argon/nitrogen and oxygen, the degradation of phenol rises. However, the extent of this rise is different for argon and nitrogen. For nitrogen the rise is ~50% while for argon the rise is rather marginal ~25%.
(3) The degradation obtained for all four gases shows a marked rise (>50% or so) with the addition of $FeSO_4{\cdot}7H_2O$ to the medium.

Illustrative simulations of radial motion of argon and oxygen bubble are shown in Figs. 4 and 5, respectively. The summary of entire simulation results (viz. temperature and pressure peak attained during transient collapse and the number of water molecules entrapped in the bubble) is given in Table 2A along with equilibrium compositions of various species generated out of dissociation of molecules present in the bubble. It can be seen that argon bubble gives much higher temperature peak during transient collapse than oxygen, nitrogen and air bubble. This is attributed to the nature of gas: argon being a monatomic gas has lower heat capacity than the other diatomic gases, due to which the bubble heats up to a greater extent, resulting in higher collapse temperature. On the other hand, the collapse temperatures of oxygen, nitrogen and air bubbles are almost similar (with a difference of ~5% or so). Conversely, the pressure peak reached at the collapse of argon bubble is lower than oxygen, nitrogen and air. It can be perceived, however, that the collapse conditions for cavitation bubbles of all four gases are beyond the critical temperature and pressure of water (647.096 K and 217.7 bar, respectively). Therefore, the equilibrium

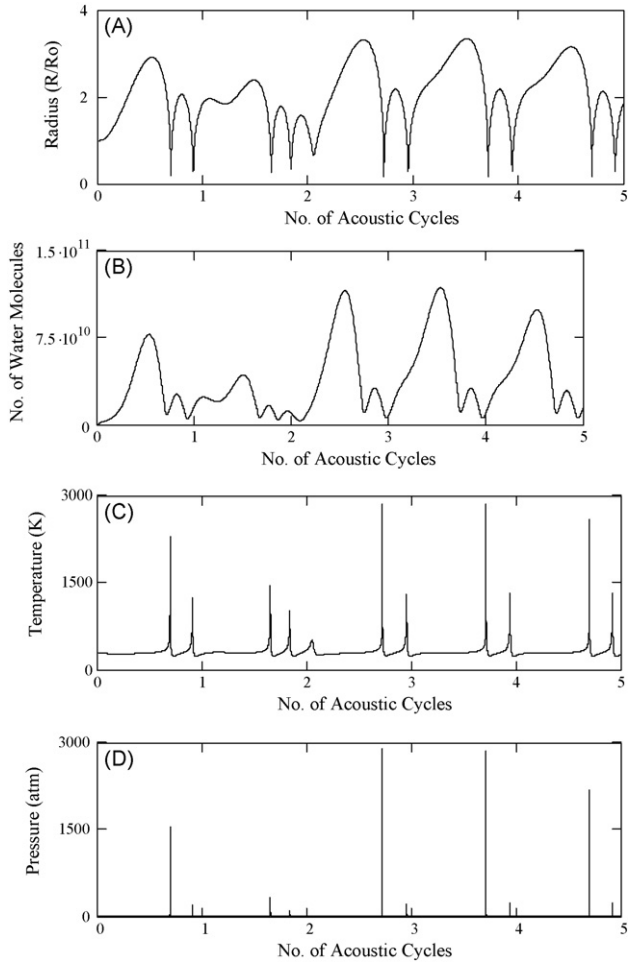


**Fig. 5.** Simulation of the radial motion of 10 μm oxygen bubble in the 100-ppm aqueous solution of phenol. Time variation of (A) normalized bubble radius ($R/R_0$); (B) number of water molecules in the bubble; (C) temperature in the bubble and (D) pressure inside the bubble.

distribution of the chemical species in the bubble is predominantly a function of temperature inside the bubble and the pressure inside the bubble has practically no influence on this distribution. The net production of four major radicals, viz. H•, •OH, O• and $HO_2$•, per bubble is given in Table 2B. The trends in the yield of these radicals are as follows:

•OH: Ar > Air > $O_2$ > $N_2$
H•: Ar > Air > $O_2$ > $N_2$
O•: Ar > Air > $O_2$ > $N_2$
$HO_2$•: Ar > $O_2$ > Air > $N_2$

An explanation to the above trends can be given as follows:

*Argon bubble*: Due to the highest temperature peak attained during transient collapse, the extent of production of all four radicals is the highest for argon bubble. For H•, O• and •OH radicals, the production rate is 2–4 orders of magnitude higher in the presence of Ar than other gases, while for $HO_2$• radical the yield is ~2 times that of oxygen bubble, which has the second highest production of these radicals among all the gases used. Due to the absence of any scavenging species in argon bubble (such as oxygen and nitrogen), the population of H• and O• radicals is also quite high.

*Air bubble*: The extent of production of all four radicals from air bubble is rather moderate. Presence of two radical scavenging species, viz. nitrogen and oxygen, in the bubble affects the distribution of radical species. The scavenging action of oxygen through reactions (R.1)–(R.7) has been explained earlier. The predominant nitrogen species produced is NO followed by $N_2O$, $NO_2$, HNO and $HNO_2$. Nitrogen present in the air bubble scavenges H•, •OH and O• radicals produced by the dissociation of entrapped water vapor through various reactions. A few representative reactions are [59]:

$$N_2 + O^\bullet \rightleftharpoons N^\bullet + NO \quad (R.12)$$

$$N_2 + {}^\bullet OH \rightleftharpoons N_2H + O^\bullet \quad (R.13)$$

$$N_2 + {}^\bullet OH \rightleftharpoons N_2O + H^\bullet \quad (R.14)$$

$$N_2 + {}^\bullet OH \rightleftharpoons NH + NO \quad (R.15)$$

$$N_2 + H^\bullet \rightleftharpoons N_2H \quad (R.16)$$

$$N_2 + H^\bullet \rightleftharpoons NH + N^\bullet \quad (R.17)$$

The nitrogen species produced in the above reactions also scavenge the radicals through various reactions. Some representative reactions are [59]:

$$N + {}^\bullet OH \rightleftharpoons NO + H^\bullet \quad (R.18)$$

$$N_2O + O^\bullet \rightleftharpoons 2NO \quad (R.19)$$

$$NO + O^\bullet \rightleftharpoons NO_2 \quad (R.20)$$

$$NH + {}^\bullet OH \rightleftharpoons NH_2 + O^\bullet \quad (R.21)$$

$$NH_2 + O^\bullet \rightleftharpoons H^\bullet + HNO \quad (R.22)$$

$$HNO + O^\bullet \rightleftharpoons NH + O_2 \quad (R.23)$$

$$HNO + O^\bullet \rightleftharpoons NO + {}^\bullet OH \quad (R.24)$$

$$HNO + {}^\bullet OH \rightleftharpoons NO + H_2O \quad (R.25)$$

It needs to be specifically mentioned that reactions (R.12)–(R.25) also occur in the bulk liquid medium due to the reaction of dissolved nitrogen with various radicals released into the bulk medium with collapse of cavitation bubble.

However, the oxygen present in the bubble reacts concurrently with nitrogen species to regenerate O• and •OH radicals through the following reactions:

$$N + O_2 \rightleftharpoons NO + O^\bullet \quad (R.26)$$

$$NO + O_2 \rightleftharpoons NO_2 + O^\bullet \quad (R.27)$$

$$NH + O_2 \rightleftharpoons HNO + O^\bullet \quad (R.28)$$

$$NH + O_2 \rightleftharpoons NO + {}^\bullet OH \quad (R.29)$$

$$N_2 + O_2 \rightleftharpoons N_2O + O^\bullet \quad (R.30)$$

Reactions (R.26)–(R.30) are also possible in the bulk liquid medium due to dissolved oxygen.

In addition, oxygen also reacts with H• and •OH radicals to yield $HO_2$• radicals through the following reactions:

$$H^\bullet + O_2 \rightleftharpoons HO_2^\bullet \quad (R.5)$$

$${}^\bullet OH + O_2 \rightleftharpoons HO_2^\bullet + O^\bullet \quad (R.8)$$

Reaction of O• radicals with oxygen molecules, however, results in loss of oxidation potential due to formation of ozone:

$$O^\bullet + O_2 \rightarrow O_3 \quad (R.31)$$

As a result of all of the above simultaneous reactions, the predominant radical species produced by air bubble is •OH followed by O•, $HO_2$• and H•—in that order.

*Oxygen bubble*: Although the temperature peak reached during transient collapse of oxygen bubble is not much different than that of an air bubble, large presence of oxygen in the bubble significantly alters the equilibrium distribution of various radical species.

**Table 2A**
Summary of the simulation results.

| Species | Parameters for simulation | | | |
|---|---|---|---|---|
| | Argon bubble | Air bubble | Oxygen bubble | Nitrogen bubble |
| | Conditions at the first compression of the bubble | | | |
| | $T_{max}$ = 3937 K | $T_{max}$ = 2478 K | $T_{max}$ = 2303 K | $T_{max}$ = 2397 K |
| | $P_{max}$ = 62.86 MPa | $P_{max}$ = 104.4 MPa | $P_{max}$ = 153.9 MPa | $P_{max}$ = 140.7 MPa |
| | $N_{Ar}$ = 1.1789E+011 | $N_{N_2}$ = 9.3053E+010 | $N_{O_2}$ = 1.1789E+011 | $N_{N_2}$ = 1.1789E+011 |
| | $N_{WT}$ = 1.51E+010 | $N_{O_2}$ = 2.4736E+010 | $N_{WT}$ = 1.4768E+10 | $N_{WT}$ = 1.4895E+010 |
| | | $N_{WT}$ = 1.09E+010 | | |
| Equilibrium composition of various species in the bubble at collapse (mole fraction) | | | | |
| $H_2O$ | 6.5869E−01 | 8.3792E−02 | 1.0988E−01 | 1.1087E−01 |
| $H_2$ | 1.3142E−01 | 3.2542E−05 | 6.2505E−06 | 9.2108E−04 |
| •OH | 1.1454E−01 | 2.1262E−03 | 1.8089E−03 | 2.8384E−04 |
| $O_2$ | 3.6855E−02 | 1.8047E−01 | 8.8788E−01 | 1.2790E−04 |
| H• | 3.8884E−02 | 4.0055E−06 | 6.2320E−07 | 1.2623E−05 |
| O• | 1.8991E−02 | 1.6967E−04 | 1.2059E−04 | 2.5566E−06 |
| HOO• | 5.4629E−04 | 1.0538E−04 | 2.7775E−04 | 4.6263E−07 |
| $H_2O_2$ | 7.1496E−05 | 7.6294E−06 | 1.8075E−05 | 2.6132E−07 |
| $O_3$ | 3.6545E−07 | 6.9832E−07 | 5.3947E−06 | 1.2032E−11 |
| $N_2$ | – | 7.1224E−01 | – | 8.8726E−01 |
| NO | – | 2.0465E−02 | – | 5.2435E−04 |
| $N_2O$ | – | 3.1507E−05 | – | 1.0453E−06 |
| $NH_3$ | – | 1.8232E−09 | – | 4.5055E−07 |
| $NO_2$ | – | 5.0932E−04 | – | 4.4288E−07 |
| HNO | – | 1.6511E−06 | – | 2.5843E−07 |
| $HNO_2$ | – | 4.6585E−05 | – | 2.9780E−07 |
| $HNO_3$ | – | 1.7913E−07 | – | 3.8363E−11 |
| N | – | 6.1669E−09 | – | 2.6931E−09 |
| NH | – | 6.1642E−10 | – | 1.9732E−09 |
| $NH_2$ | – | 7.3593E−10 | – | 1.9954E−08 |
| $NO_3$ | – | 3.9991E−08 | – | 9.8969E−13 |
| $N_3$ | – | 4.5001E−11 | – | 3.6032E−11 |
| $N_2H_2$ | – | 8.6303E−13 | – | 2.8980E−11 |
| $N_2O_3$ | – | 6.3221E−09 | – | 1.9798E−13 |
| $N_2O_4$ | – | 1.6757E−11 | – | – |
| $N_2H_4$ | – | – | – | 1.8212E−14 |
| $N_2O_5$ | – | 3.4491E−13 | – | – |

*Note*: $T_{max}$, temperature peak reached in the bubble at the time of first collapse; $P_{max}$, pressure peak reached in the bubble at the time of first collapse; $N_{WT}$, number of water molecules trapped in the bubble at the instance of first collapse; $N_{O_2}$, number of oxygen molecules in the bubble (for air and oxygen bubbles); $N_{Ar}$, number of argon molecules in the bubble; $N_{N_2}$, number of nitrogen molecules in the bubble.

Scavenging of H• radicals by oxygen molecules reduces the mole fraction of H• significantly (reactions (R.4) and (R.5)), with concurrent rise in quantity of $HO_2$• radicals (reaction (R.5)). O• radicals formed out of dissociation of oxygen molecules react with oxygen to form ozone (reaction (R.31)). Moreover, $HO_2$• radicals can combine to form $H_2O_2$ through the following reaction:

$$2HO_2^{\bullet} \rightleftharpoons H_2O_2 + O_2 \quad \text{(R.32)}$$

It can be seen from Table 2A that the mole fraction of $H_2O_2$ and $O_3$ for oxygen bubble is one order of magnitude higher than air bubble. Both reactions (R.31) and (R.32) result in loss of oxidation potential. The overall result of all simultaneous reactions is the production of •OH and $HO_2$• as the predominant radical species.

*Nitrogen bubble*: Although the temperature peak attained during collapse of nitrogen bubble is higher than the oxygen bubble, the radical production is significantly less. Except for H• radical, the yield of other radicals (viz. O•, •OH and $HO_2$•) is 1–3 order(s) of magnitude smaller. This effect is attributed to extensive scavenging of radicals by nitrogen molecules (through reactions (R.12)–(R.25)). The absence of oxygen in the bubble has two effects on the equilibrium composition: first, low yield of $HO_2$• radicals which form out of scavenging of H• radicals by oxygen (reaction (R.4)), and secondly, larger population of H• radicals in the bubble during transient collapse as a consequence of first effect.

Simultaneous assessment of the simulation results and experimental results in different categories as stated earlier reveals some interesting mechanistic features of the sonochemical degradation of phenol, as described below:

- *Category I* (*continuous bubbling of Ar/$N_2$/$O_2$/air*)
  - The extent of degradation obtained for air and argon as bubbling gas is almost equal, although the extent of radical production differs by an order of magnitude. This effect is explained in terms of variation in the dissolved oxygen content, and hence, the extent of radical scavenging in the liquid medium with bubbling of the gas through reactions (R.1)–(R.8). In case of bubbling

**Table 2B**
Net production of various radicals per bubble.

| Parameter | Argon bubble | Air bubble | Oxygen bubble | Nitrogen bubble |
|---|---|---|---|---|
| $N_T$ | 1.3299E+011 | 1.2879E+011 | 1.3266E+011 | 1.3279E+011 |
| $N_{OH}$ | 1.5233E+09 | 2.7383E+08 | 2.3997E+08 | 3.7683E+07 |
| $N_H$ | 5.1711E+09 | 5.1587E+05 | 8.2672E+04 | 1.6761E+06 |
| $N_O$ | 2.5256E+09 | 2.1852E+07 | 1.5997E+07 | 3.3948E+05 |
| $N_{HO_2}$ | 7.2651E+09 | 1.3572E+07 | 3.6846E+07 | 6.1430E+04 |

*Note*: The number format is as follows: 6.5869E−01 should be read as $6.5869 \times 10^{-1}$. Nomenclature: $N_T$, total number of molecules present in the bubble at transient collapse; $N_{OH}$, number of OH radicals present in the bubble at transient collapse; $N_H$, number of H radicals present in the bubble at transient collapse; $N_O$, number of O radicals present in the bubble at transient collapse; $N_{HO_2}$, number of $HO_2$ radicals present in the bubble at transient collapse.

of air, the oxygen in air dissolves in the liquid medium. Hence, the concentration of the dissolved oxygen is maintained nearly to the saturation level, which helps in effective scavenging of radicals. On the other hand, bubbling of argon strips out dissolved oxygen present in the medium (refer to Fig. 3), which annihilates the scavenging of radicals. Therefore, the radical recombination phenomenon dominates causing loss in oxidation potential, resulting in a lower degradation of phenol.

- Least degradation with nitrogen as the bubbling gas is due to the combined result of lower rate of production of radicals coupled with the stripping away of dissolved oxygen in the medium, due to which radical scavenging is hampered. The probability of phenol–radical interaction is, thus, very sparse and most of the radicals undergo recombination.
- Although the net production of radicals per cavitation bubble for air and oxygen does not differ much, the degradation with oxygen is much higher than air. Higher degradation for oxygen as bubbling gas is a result of effective scavenging of radicals outside the bubble by oxygen molecules dissolved in the medium, as well as tiny bubbles of oxygen that remain suspended in the medium during bubbling of oxygen (through reactions (R.1)–(R.8) discussed earlier). Moreover, the dissolved oxygen content of the bulk medium stays at saturation level all along sonication, which gives maximum scavenging effect resulting in highest degradation.

- *Category II* (*alternate bubbling of Ar/$N_2$ and oxygen*)With alternate bubbling of oxygen and nitrogen or argon, the extent of degradation shows marginal enhancement. One can easily perceive that intermittent bubbling of $O_2$ (at a relatively high rate of $2.778 \times 10^{-3}$ mL/s or 10 L/h) for 300 s (5 min) during silent period of the reaction will increase the dissolved oxygen content of the medium, close to the saturation level of 0.25 mM (8 ppm). With this, the radical scavenging phenomenon is restored temporarily. However, the dissolved oxygen content of the medium drops rapidly with bubbling of $N_2$ or Ar in the ensuing sonication period of 900 s (15 min). As seen in Fig. 3, the dissolved oxygen content reduces from a saturation value of 0.25 mM (8 ppm) to ~0.063 mM (2 ppm) in 900 s (15 min). Accordingly, the rise in degradation of phenol is only marginal in second category of experiments.

- *Category III* (*continuous bubbling of Ar/$N_2$/$O_2$/Air with $FeSO_4 \cdot 7H_2O$ added to the liquid medium*)Addition of $FeSO_4 \cdot 7H_2O$ to the aqueous solution of pollutant results in a marked rise in the degradation obtained. Although the trend in the degradation with different gases remains same as category I, the absolute values of the degradation are higher. Several factors contribute to this effect: (1) the scavenging action of $FeSO_4 \cdot 7H_2O$ is due to the reaction of $Fe^{2+}$ ions with $H_2O_2$ generated in the medium as a result of recombination of $^{\bullet}OH$ radicals (reaction (R.6)). In the process $Fe^{2+}$ ions are oxidized to $Fe^{3+}$. Being an ionic species the reactivity of $Fe^{2+}$ is far higher than oxygen, which exists as molecular species; (2) bubbling of gas (in case of nitrogen and argon) does not reduce the concentration of this species, as it is not stripped out of the medium; (3) $Fe^{2+}$ is continuously regenerated in the medium due to reaction of $Fe^{3+}$ ion with hydrogen peroxide and $HO_2^{\bullet}$ radicals (per reactions (R.10) and (R.11)). It should be noted that the $H_2O_2$ generated by the cavitation bubble in equilibrium proportion among various species generated out of dissociation of water vapor is negligible (with mole fraction $<10^{-6}$ for bubbles of all four gases). Thus, the $H_2O_2$ that reacts with $Fe^{2+}$ is mainly generated due to recombination of $^{\bullet}OH$ radicals. The overall result is far more effective scavenging of radicals in the medium giving higher degradation. It is interesting to note that in the third category of experiments, the degradation with air and oxygen bubbling is still higher than with argon bubbling, although the radical production by an argon bubble is one order of magnitude higher than air and oxygen bubbles, as mentioned earlier. We attribute this anomaly to the additive effect of $Fe^{2+}$ and oxygen for radical scavenging.

## 6. Conclusion

In the present investigation, we have tried to reveal interesting facets of the overall physics and mechanism of the sonochemical degradation of phenol, which have vital involvement in the enhancement of the degradation rates. With experiments under different reaction conditions and a mathematical model for the radial motion of cavitation bubbles, we have shown the relative influence of two physical processes, viz. radical generation (using monatomic and diatomic gases, viz. argon, nitrogen, oxygen and air) and radical scavenging (using molecular and ionic species, viz. oxygen and $Fe^{2+}$), on the sonochemical degradation of phenol. As stated earlier, the degradation of phenol occurs in the bulk liquid medium due to hydroxylation reaction induced by $^{\bullet}OH$ radicals generated from cavitation bubble. This is a consequence of low vapor pressure of phenol (due to which it does not evaporate into the cavitation bubble) and the hydrophilic nature of the phenol molecule.

Unlike conventional chemical reactions where the rate is determined by the concentration of reactants, the rate of sonochemical degradation of phenol (with phenol and $^{\bullet}OH$ radical as the reactants) seems to be governed by the rate of scavenging of the radicals. This effect originates from low concentration of phenol in the liquid medium, due to which the probability of interaction between radicals and phenol molecules becomes an important factor influencing the overall degradation. The scavenging phenomenon increases this probability and gives higher degradation. Moreover, the concentration of the radical scavenging species is another important factor affecting the degradation. Atypically, monatomic gas such as argon, which is generally used for increasing the yield of the sonochemical reactions, is found to give low degradation. This is an outcome of the counterproductive effect of bubbling of argon on scavenging phenomena due to stripping out of dissolved oxygen from the liquid medium. On the other hand, the ionic species $Fe^{2+}$ is found to be far more efficient for radical scavenging even at very low concentration levels. This is attributed to faster reactivity of $Fe^{2+}$ ions and uniform concentration of the $Fe^{2+}$ ions during sonication.

On a whole, the results of this study give a mechanistic assessment of various techniques that can enhance the sonochemical degradation of phenol. It should be noted that the approach presented in this paper could also form a framework for study in intensification of sonochemical degradation of any other non-volatile organic pollutant, which has similar degradation chemistry (i.e. hydroxylation route) as phenol.

## Acknowledgments

Authors gratefully acknowledge valuable suggestions for the analysis of bubble–bulk interfacial region from Prof. Franz Grieser and Dr. M. Ashok Kumar (University of Melbourne, Australia) and Prof. A.B. Pandit and Dr. P.S. Bapat (UICT, Mumbai, India). Authors also thank Prof. Andrea Prosperetti (Johns Hopkins University, USA), Dr. Brian Storey (Franklin W. Olin College of Engineering, USA) and Dr. Rudiger Toegel (University of Twente, Netherlands) for their help in the bubble dynamics modeling. This work was financially supported by Department of Science and Technology (DST), Government of India under Fast Track Scheme for Young Scientists.

## References


[1] E.J. Hart, A. Henglein, Free radical and free atom reactions in the sonolysis of aqueous iodide and formate solutions, J. Phys. Chem. 89 (20) (1985) 4342–4347.
[2] E.J. Hart, A. Henglein, Sonochemistry of aqueous solutions: hydrogen–oxygen combustion in cavitation bubbles, J. Phys. Chem. 91 (13) (1987) 3654–3656.
[3] K.S. Suslick, Sonochemistry, Science 247 (1990) 1439–1445.
[4] J. Berlan, F. Trabelsi, H. Delmas, A.M. Wilhelm, J.F. Petrignani, Oxidative degradation of phenol in aqueous media using ultrasound, Ultrason. Sonochem. 1 (2) (1994) S97–S102.
[5] P.R. Gogate, S. Mujumdar, J. Thampi, A.M. Wilhelm, A.B. Pandit, Destruction of phenol using sonochemical reactors: scale-up aspects and comparison of novel configuration with conventional reactors, Sep. Purif. Technol. 34 (2004) 25–34.
[6] C. Petrier, A. Francony, Ultrasonic wastewater treatment: incidence of ultrasonic frequency on the rate of phenol and $CCl_4$ degradation, Ultrason. Sonochem. 4 (4) (1997) 295–300.
[7] C. Petrier, M.F. Lamy, A. Francony, A. Benahcene, B. David, V. Renaudin, N. Gondrexon, Sonochemical degradation of phenol in dilute aqueous solutions: comparison of the reaction rates at 20 and 487 kHz, J. Phys. Chem. 98 (1994) 10514–10520.
[8] M.H. Entezari, C. Petrier, A combination of ultrasound and oxidative enzyme: sonoenzyme degradation of phenols in a mixture, Ultrason. Sonochem. 12 (4) (2005) 283–288.
[9] M.H. Entezari, C. Petrier, P. Devidal, Sonochemical degradation of phenol: a comparison of classical equipment with a new cylindrical reactor, Ultrason. Sonochem. 10 (2) (2003) 103–108.
[10] N.N. Mahamuni, A.B. Pandit, Effect of additives on ultrasonic degradation of phenol, Ultrason. Sonochem. 13 (2006) 165–174.
[11] F. Trabelsi, H. Ait-Lyazidi, B. Ratsimba, A.M. Wilhelm, H. Delmas, P.L. Fabre, J. Berlan, Oxidation of phenol in wastewater by sonochemistry, Chem. Eng. Sci. 51 (10) (1996) 1857–1865.
[12] Y. Chen, P. Smirniotis, Enhancement of photocatalytic degradation of phenol and chlorophenols with ultrasound, Ind. Eng. Chem. Res. 41 (24) (2002) 5958–5965.
[13] J. Seymour, R.B. Gupta, Oxidation of aqueous pollutants using ultrasound: salt induced enhancement, Ind. Eng. Chem. Res. 36 (9) (1997) 3453–3457.
[14] T.M. Lesko, Chemical Effects of Acoustic Cavitation. Ph.D. Thesis, California Institute of Technology, Pasadena, 2004.
[15] M. Kubo, K. Matsuoka, A. Takahashi, N. Shibasaki-Kitakawa, T. Yonemoto, Kinetics of ultrasonic degradation of phenol in presence of $TiO_2$ particles, Ultrason. Sonochem. 12 (4) (2005) 263–269.
[16] S. Okouchi, O. Nojima, T. Arai, Cavitation induced degradation of phenol by ultrasound, Water Sci. Technol. 26 (9–11) (1992) 2053–2056.
[17] N. Serpone, R. Terzian, P. Colarusso, Sonochemical oxidation of phenol and three of its intermediates in aqueous media: catechol, hydroquinone and benzoquinone: kinetics and mechanistic aspects, Res. Chem. Intermediat. 18 (2–3) (1992) 183–202.
[18] C. Wu, X. Liu, D. Wei, J. Fan, L. Wang, Photosonochemical degradation of phenol in water, Water Res. 35 (16) (2001) 3927–3933.
[19] M. Papadaki, R.J. Emery, M.A. Abu-Hassan, A. Diaz-Bustos, I.S. Metcalfe, D. Mantzarinos, Sonocatalytic oxidation process for the removal of contaminants containing aromatic ring from aqueous effluents, Sep. Purif. Technol. 34 (1–3) (2004) 35–42.
[20] Y. Takizawa, M. Akama, N. Yoshihara, O. Nojima, K. Arai, S. Okouchi, Hydroxylation of phenolic compounds under conditions of ultrasound in aqueous solutions, Ultrason. Sonochem. 3 (1996) S201–S204.
[21] W. Zheng, M. Michelle, M.A. Tarr, Enhancement of degradation of phenol using hydrogen atom scavengers, Ultrason. Sonochem. 12 (4) (2004) 313–317.
[22] Y. Jiang, C. Petrier, T. David Waite, Effect of pH on the ultrasonic degradation of ionic aromatic compounds in aqueous solutions, Ultrason. Sonochem. 9 (3) (2002) 163–168.
[23] B.D. Storey, A.J. Szeri, Water vapor, sonoluminescence and sonochemistry, Proc. R. Soc. Lond. Ser. A 456 (2000) 1685–1709.
[24] R. Toegel, B. Gompf, R. Pecha, D. Lohse, Does water vapor prevent upscaling sonoluminescence? Phys. Rev. Lett. 85 (2000) 3165–3168.
[25] A. Henglein, The acceleration of chemical reaction induced by ultrasound in solutions of oxygen noble gas mixtures, Naturwissenschaften 43 (1956) 277.
[26] A. Henglein, Hydrogen peroxide formation by ultrasound in aqueous solutions of mixtures of hydrogen, argon and oxygen, Naturwissenschaften 44 (1957) 179.
[27] I. Hua, M.R. Hoffmann, Optimization of ultrasonic irradiation as an advanced oxidation technology, Environ. Sci. Technol. 31 (1997) 2237–2243.
[28] P.S. Bapat, P.R. Gogate, A.B. Pandit, Theoretical analysis of sonochemical degradation of phenol and its chloro-derivatives, Ultrason. Sonochem. 14 (1) (2008) 564–570.
[29] A.W. Adamson, A.P. Gast, Physical Chemistry of Surfaces, John Wiley and Sons, NY, 1997.
[30] P. Joos, G. Serrien, Adsorption kinetics of lower alkanols at the air/water interface: effect of structure makers and structure breakers, J. Colloid Interf. Sci. 127 (1) (1989) 97–103.
[31] T. Sivasankar, A.W. Paunikar, V.S. Moholkar, Mechanistic approach to enhancement of the yield of a sonochemical reaction, AIChE J. 53 (5) (2007) 1132–1143.
[32] V. Kamath, A. Prosperetti, F.N. Egolfopoulos, A theoretical study of sonoluminescence, J. Acoust. Soc. Am. 94 (1993) 248–260.
[33] D.V. Prasad Naidu, R. Rajan, R. Kumar, K.S. Gandhi, V.H. Arakeri, S. Chandrasekaran, Modeling of a batch sonochemical reactor, Chem. Eng. Sci. 49 (1994) 877–888.
[34] K. Yasui, Alternative model for single-bubble sonoluminescence, Phys. Rev. E 56 (1997) 6750–6760.
[35] K. Yasui, Chemical reactions in a sonoluminescing bubble, J. Phys. Soc. Jpn. 66 (1997) 2911–2920.
[36] S. Sochard, A.M. Wilhelm, H. Delmas, Modeling of free radicals production in a collapsing gas–vapor bubble, Ultrason. Sonochem. 4 (1997) 77–84.
[37] C. Gong, D.P. Hart, Ultrasound induced cavitation and sonochemical yields, J. Acoust. Soc. Am. 104 (1998) 2675–2682.
[38] W.C. Moss, D.A. Young, J.A. Harte, J.L. Levalin, B.F. Rozsnyai, G.B. Zimmerman, I.H. Zimmerman, Computed optical emissions from sonoluminescing bubbles, Phys. Rev. E 59 (1999) 2986–2992.
[39] S. Fujikawa, T. Akamatsu, Effects of the non-equilibrium condensation of vapor on the pressure wave produced by the collapse of a bubble in a liquid, J. Fluid Mech. 97 (1980) 481–512.
[40] H.Y. Kwak, J.-H. Na, Hydrodynamic solutions for sonoluminescing gas bubble, Phys. Rev. Lett. 77 (1996) 4454–4457.
[41] H.Y. Kwak, J.-H. Na, Physical processes for single bubble sonoluminescence, J. Phys. Soc. Jpn. 66 (1997) 3074–3083.
[42] H.Y. Kwak, H. Yang, An aspect of sonoluminescence from hydrodynamic theory, J. Phys. Soc. Jpn. 64 (1995) 1980–1992.
[43] V.I. Ilyichev, V.L. Koretz, N.P. Melnokov, Spectral characteristics of acoustic cavitation, Ultrasonics 27 (1989) 357–361.
[44] R. Rajan, R. Kumar, K.S. Gandhi, Modeling of sonochemical oxidation of the water–KI–$CCl_4$ system, Chem. Eng. Sci. 53 (1998) 255–271.
[45] B.D. Storey, A.J. Szeri, A reduced model of cavitation physics for use in sonochemistry, Proc. R. Soc. Lond. Ser. A 457 (2001) 1685–1700.
[46] A. Prosperetti, A. Lezzi, Bubble dynamics in a compressible liquid. Part 1. First order theory, J. Fluid Mech. 168 (1986) 457–477.
[47] C.E. Brennen, Cavitation and Bubble Dynamics, Oxford University Press, Oxford, 1995.
[48] S.J. Krishnan, P. Dwivedi, V.S. Moholkar, Numerical investigation into the chemistry induced by hydrodynamic cavitation, Ind. Eng. Chem. Res. 45 (2006) 1493–1504.
[49] K.S. Kumar, V.S. Moholkar, Conceptual design of a novel hydrodynamic cavitation reactor, Chem. Eng. Sci. 62 (2007) 2698–2711.
[50] J.O. Hirschfelder, C.F. Curtiss, R.B. Bird, Molecular Theory of Gases and Liquids, Wiley, NY, 1954.
[51] R.C. Reid, J.M. Prausnitz, B.E. Poling, Properties of Gases and Liquids, McGraw-Hill, NY, 1987.
[52] C.R. Wilke, A viscosity equation for gas mixtures, J. Chem. Phys. 18 (1950) 517–519.
[53] H. Odishaw, E.U. Condon, Handbook of Physics, McGraw-Hill, NY, 1958.
[54] W.H. Press, S.A. Teukolsky, B.P. Flannery, W.T. Vetterling, Numerical Recipes, Cambridge University Press, NY, 1992.
[55] T.J. Mason, J.P. Lorimer, Theory, Application and Uses of Ultrasound in Chemistry, Ellis Horwood, NY, 1989.
[56] A. Prosperetti, K.W. Commander, Linear pressure waves in bubbly liquids: comparison between theory and experiments, J. Acoust. Soc. Am. 83 (1989) 502–514.
[57] F.R. Young, Cavitation, McGraw Hill, London, 1989.
[58] G. Eriksson, Thermodynamic studies of high temperature equilibria—XII: SOLGAMIX, a computer program for calculation of equilibrium composition in multiphase systems, Chem. Scripta 8 (1975) 100–103.
[59] R. Toegel, Reaction–Diffusion Kinetics of a Single Sonoluminescing Bubble (Ph.D. Dissertation), Twente University Press, Enschede, 2002.
[60] R. Toegel, D. Lohse, Phase diagrams for sonoluminescing bubbles: A comparison between experiment and theory, J. Chem. Phys. 118 (4) (2003) 1863–1875.